Supporting Information for: Determination of Biomembrane Bending Moduli in Fully Atomistic Simulations.

Molecular Dynamics Simulation Details

All simulations were performed with the Chemistry at HARvard Molecular Mechanics (CHARMM) program and CHARMM36 force field. Non-bonded interactions in CHARMM36 are modeled with Coulombic and 6-12 Lennard-Jones potentials, while bonded interactions are maintained through bond length, bond angle, torsional angle, and improper dihedral terms. Lennard-Jones potentials were brought to zero by a force-switch over the interval 8- 12 Å. Electrostatics were evaluated using Particle Mesh Ewald (PME) summation where short range interactions (≤ 12 Å) were tabulated in direct-space while long-range electrostatics (> 12 Å) were tabulated in reciprocal space using Fast Fourier Transforms (FFT). Each system contained 648 lipids (324 lipids per leaflet) and between 19701-21681 water molecules which resulted in unit cells of 142-148 Å in xy and 68-74 Å in z. An NPT ensemble was maintained in each of the three membrane systems which were comprised of either 1,2-dipalmitoyl-*sn*-glycero-3-phosphatidylcholine (DPPC), 1,2-dioleoyl-*sn*-glycero-3-phosphatidylcholine (DOPC), or 1,2-dioleoyl-*sn*-glycero-3-phosphatidylethanolamine (DOPE). The DOPC and DOPE simulations used the c38b1 CHARMM version with DOMDEC,[1] while the DPPC simulation, run much earlier, used c35b4. Extended system pistons with a mass of 1000 amu were utilized as a barostat to maintain 1 atm of pressure in xy and z, while a Nosé-Hoover thermostat was used to fix temperature at either 50° C for DPPC, or at 24.9° C for DOPC and DOPE so that all three lipid species could be simulated in the fluid phase. Trajectories were carried out using the leapfrog Verlet integrator with a timestep of 1 fs for a total of 110 ns for DPPC, 170 ns for DOPC, and 140 ns for DOPE; the first 10 ns were dropped in each case. Periodic boundary conditions were applied in all three dimensions.

Simulation Analysis Details

The following procedure is adapted from that described in Appendix C of Ref. 2. The present work is concerned primarily with analysis of the 2D lipid orientation vector field, $\mathbf{n}(\mathbf{r})=\mathbf{n}(x,y)$, and secondarily with the bilayer height scalar field, $h(\mathbf{r})=h(x,y)$. Explicit instructions for the extraction of the power spectra $< |h_q|^2 >$, $< |\hat{n}_q^{\parallel}|^2 >$ and $< |\hat{n}_q^{\perp}|^2 >$ appearing in Eqs. 1,2 and 3 of the main text are presented here. Fields are obtained using a real-space gridding procedure applied to the simulation data. Individual lipids in a given time step are sorted into a square MxM grid in the (x, y) plane where M=12. Here (x_j, y_j, z_j) refers to the position of the vector tail of the *j*th lipid as displayed in Fig. 1 (corresponding either to the midpoint between phosphorus and glycerol C2 atoms for the lipid orientation definition employed in the main text, or to the alternate molecular definitions discussed below). $\mathbb{m}_j$ is the three-dimensional unit vector pointing in the direction from (x_j, y_j, z_j) to the corresponding vector head position in Fig. 1 (which is located at either the midpoint between the two terminal methyl carbons of the lipid tails for the main text definition, or to the alternate molecular definitions discussed below). The discretization and analysis procedure consists of the following steps:

(a) Determine the mean z-coordinate of all vector tail points: $\bar{z} = \frac{1}{N}\sum_{j=1}^{N} z_j$. This quantity corresponds to the bilayer center. N = 648 is the total number of lipids in the simulation.

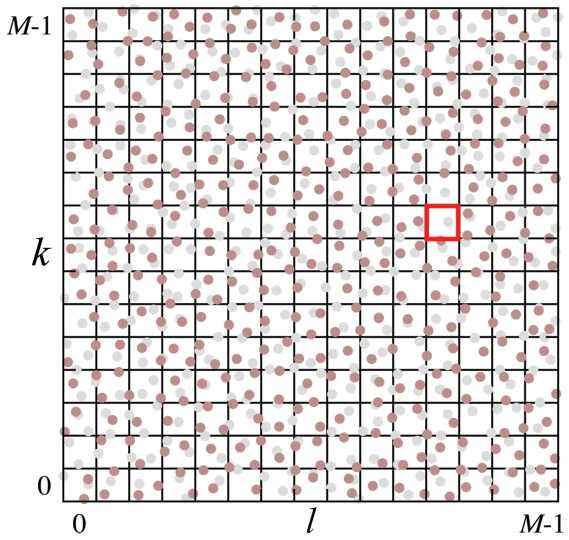

Figure S1. Schematic of lipid assignment to a MxM grid. Filled circles represent lipid orientation vector tail points (brighter: lipid in the lower monolayer; darker: lipid in upper monolayer). The highlighted square is an example of a patch that does not contain any lipids in the upper monolayer ($N_{kl}^{(1)} = 0$).

(b) Divide lipids into upper and lower monolayers on the basis of position relative to $\overline{z}$:

$$\text{upper monolayer:} \qquad z_j > \overline{z}$$

$$\text{lower monolayer:} \qquad z_j < \overline{z}.$$

Once the lipids have been assigned to each monolayer, they are analyzed separately in the following steps (c-e).

(c) Assign lipids to a grid point (Figure S1). The *j*th lipid is assigned to the patch with indices (k, l), where k, l = 0...M−1 based on the xy-coordinates of its orientation vector tail point according to the expression

$$(k,l)_j = \left(\left\lfloor x_j \frac{M}{L} \right\rfloor, \left\lfloor y_j \frac{M}{L} \right\rfloor\right), \tag{S1}$$

where ⌊... ⌋ is the floor function and L the box length in xy. (Assigning the averages of each patch to its lower left corner rather than its center amounts to an overall translation, which has no effect on the measured spectra in Fourier space.)

(d) Calculate the average z-coordinate relative to the bilayer center of each monolayer patch (z_{kl}), and the average lipid orientation vector of each monolayer patch ($\mathbb{m}_{kl}$), in terms of the number of lipids within that patch N_{kl}:

$$z_{kl} = \frac{1}{N_{kl}} \sum_j' z_j - \overline{z}, \tag{S2}$$

$$\mathbb{m}_{kl} = \frac{1}{N_{kl}} \sum_j' \mathbb{m}_j$$

where Σ' indicates summation only over the N_{kl} lipids in monolayer patch (k, l). The corresponding 2D orientation vector of monolayer patch *(k,l)*, $\boldsymbol{n_{kl}}$, is obtained as the projection of $\mathbb{m}_{kl}$ onto the x,y plane.

(e) If a monolayer patch contains no lipids (N_{kl} = 0) as in the red square of Figure S1, then a simple interpolation is performed. For example, the monolayer z-coordinate is calculated as a weighted average from the nearest-neighbor grid points located at <k, l> = ($k \pm 1$, $l \pm 1$):

$$z_{kl} = \frac{\sum_{<k,l>} N_{<k,l>} z_{<k,l>}}{\sum_{<k,l>} N_{<k,l>}}. \quad \text{(S3)}$$

An analogous interpolation is carried out for the 2D orientation vectors. This method assumes that no two neighboring patches within the same monolayer are empty. The grid spacing M=12 is sufficiently dense to satisfy this criterion.

(f) Take the Fast Fourier Transform (FFT) of z_{kl} and $\boldsymbol{n_{kl}}$ to obtain $z_{\boldsymbol{q}}$ and $\boldsymbol{n_q}$ for each monolayer. The vector index $\boldsymbol{q}$ indicates the 2D Fourier wavevector. Combine the monolayer z fields and orientation fields to yield the bilayer height field and bilayer orientation field.

$$h_{\boldsymbol{q}} = \frac{z_{\boldsymbol{q}}^{(1)} + z_{\boldsymbol{q}}^{(2)}}{2} \quad \text{(S4)}$$

$$\hat{\boldsymbol{n}}_{\boldsymbol{q}} = \frac{\boldsymbol{n}_{\boldsymbol{q}}^{(1)} - \boldsymbol{n}_{\boldsymbol{q}}^{(2)}}{2} \quad \text{(S5)}$$

where the (1) and (2) superscripts refer to the top and bottom monolayers, respectively.

(g) Calculate the longitudinal and transverse components of the bilayer orientation fields $\{\hat{n}_q^{\perp}, \hat{n}_q^{\parallel}\}$ using the transformation:

$$\begin{pmatrix} \hat{n}_q^{\parallel} \\ \hat{n}_q^{\perp} \end{pmatrix} = \frac{1}{q} \begin{pmatrix} q_x & q_y \\ -q_y & q_x \end{pmatrix} \begin{pmatrix} \hat{n}_q^{x} \\ \hat{n}_q^{y} \end{pmatrix} \quad \text{(S6)}$$

(h) Take the square modulus and average over time steps (separated here by 0.5 ns) to acquire the power spectra $< |h_q|^2 >$, $< |\hat{n}_q^{\parallel}|^2 >$ and $< |\hat{n}_q^{\perp}|^2 >$.

(i) Obtain spectra which only depend on the length of q by averaging data sets over $\boldsymbol{q}'$ values for which $|\boldsymbol{q}'|$=q.

(j) Membrane moduli are extracted by fitting the simulated power spectra to the theoretical predictions of eq 2. For comparisons to the height field approach based on eq 3 (see "Alternate Analysis Methods and a Test of Box Size Dependence" below), the tilt modulus is first extracted via analysis of the transverse orientation spectrum. The contribution of tilting to eq 3 may then be subtracted off, and the bending modulus obtained by fitting the corrected spectrum to eq 1. (See Fig. S6).

Modulus Standard Error Obtained through Block Averages

To determine statistical error in our calculations, we compared K_c, K_θ, and K_{tw} across individual 10 ns blocks which, when summed, make up the entire simulation trajectory. This allows us to both calculate a standard error and observe the rate of convergence for each modulus as it is extracted from all-atom molecular dynamics simulations. The results for each system are listed below. The first 10 nanoseconds were dropped for all subsequent statistical analysis.

Table S1. Block averages of membrane moduli in a DPPC membrane

Time (ns)	**0-10**	**10-20**	**20-30**	**30-40**	**40-50**	**50-60**	**60-70**	**70-80**	**80-90**	**90-100**	**100-110**	**Avg.**	**StErr**
K_c (x 10^{-20} J)	13.0	13.0	17.7	16.6	15.2	15.2	15.6	15.7	14.7	15.8	18.2	15.8	0.5
K_θ (x 10^{-20} J/nm^2)	5.4	4.5	4.9	5.3	4.4	4.36	5.9	5.5	4.6	4.9	4.7	5.0	0.2
K_{tw} (x 10^{-20} J)	2.0	2.1	2.0	1.8	2.3	2.2	1.8	2.0	1.9	1.9	2.1	2.0	0.1

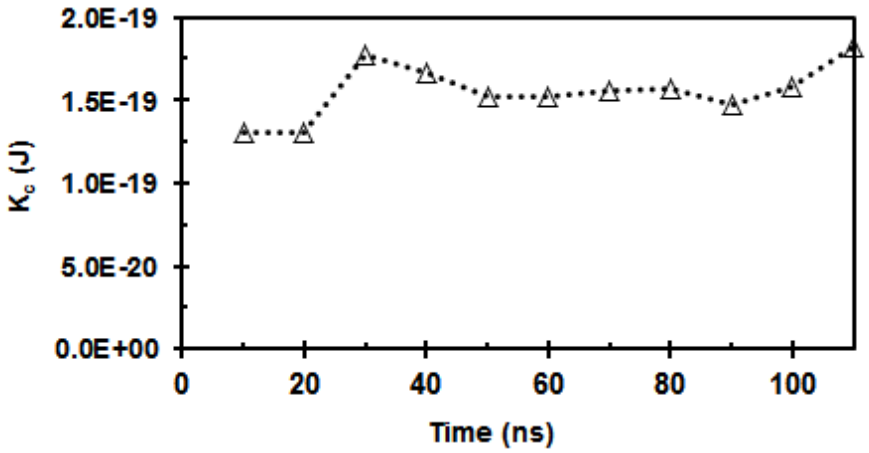

Figure S2. 10 ns block averages of K_c for DPPC

Table S2. Block averages of membrane modulii in a DOPC membrane

Time (ns)	**0-10**	**10-20**	**20-30**	**30-40**	**40-50**	**50-60**	**60-70**	**70-80**	**80-90**	**90-100**
K_c (x 10^{-20} J)	11.8	10.0	11.3	13.8	11.9	13.6	11.2	11.1	11.5	11.0
K_θ (x 10^{-20} J/nm^2)	5.8	6.2	6.8	5.6	6.1	8.5	7.6	7.7	7.0	7.1
K_{tw} (x 10^{-20} J)	1.7	1.2	0.9	1.3	1.1	0.6	0.6	0.8	1.1	1.0
Time (ns)	**100-110**	**110-120**	**120-130**	**130-140**	**140-150**	**150-160**	**160-170**	**Avg.**	**StErr**	
K_c (x 10^{-20} J)	12.6	13.1	11.0	12.5	11.8	9.6	8.9	11.5	0.3	
K_θ (x 10^{-20} J/nm^2)	6.7	6.1	5.7	7.1	7.1	7.7	6.2	6.8	0.2	
K_{tw} (x 10^{-20} J)	1.0	1.4	1.2	1.2	1.0	0.9	1.1	1.0	0.1	

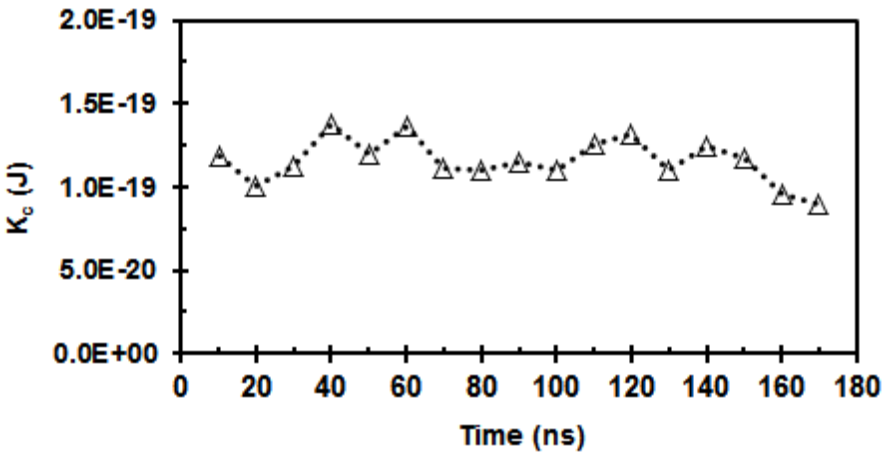

Figure S3. 10 ns block averages of K_c for DOPC

Table S3. Block averages of membrane modulii in a DOPE membrane

Time (ns)	**0-10**	**10-20**	**20-30**	**30-40**	**40-50**	**50-60**	**60-70**	**70-80**	**80-90**	**90-100**
K_c (x 10^{-20} J)	11.3	9.4	11.5	11.5	13.3	12.3	12.8	11.2	13.1	11.5
K_θ (x 10^{-20} J/nm^2)	8.5	9.7	7.3	8.4	10.5	9.6	8.7	10.6	7.3	8.8
K_{tw} (x 10^{-20} J)	2.1	1.4	1.9	1.3	1.0	1.2	1.5	0.9	2.0	1.4

Time (ns)	**100-110**	**110-120**	**120-130**	**130-140**	**Avg.**	**StErr**
K_c (x 10^{-20} J)	11.1	10.7	13.5	10.7	11.7	0.3
K_θ (x 10^{-20} J/nm^2)	9.2	8.5	6.0	7.4	8.6	0.4
K_{tw} (x 10^{-20} J)	1.0	1.6	2.6	1.9	1.5	0.1

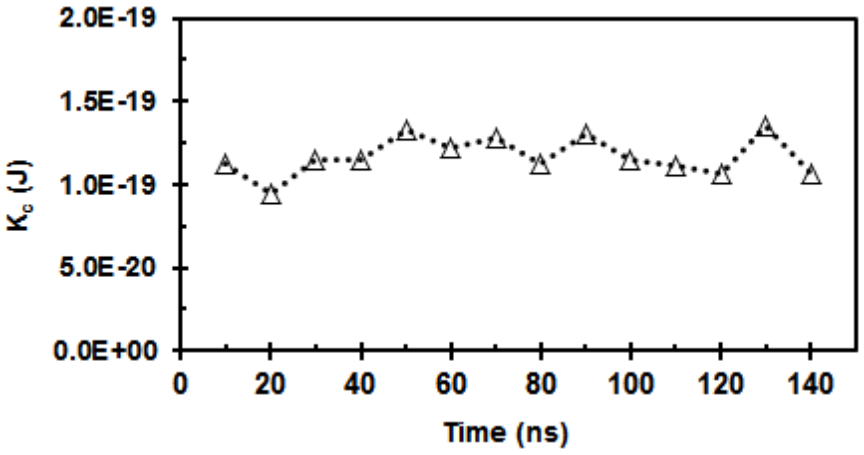

Figure S4. 10 ns block averages of K_c for DOPE

The standard errors listed in Tables S1-S3 are cited in Table 1; the average moduli are not. The moduli reported in Table 1 were obtained by fitting the power spectra from the full simulation to eq 2. The "Avg." columns in Tables S1-S3 were obtained by averaging the results from the individual blocks, with the results from each block obtained by fitting the power spectra associated with the block. The fitting process is non-linear and it is not expected that the two averaging procedures coincide exactly. (The average of a function of a random variable is not the same thing as the function of the average of the variable.) The two moduli values (full simulation vs. block average) are identical within the reported standard errors; we call attention to these small differences only to avoid possible confusion regarding the apparent inconsistencies between Tables S1-S3 and Table 1 of the main text.

Membrane Modulus Values using Alternate Definitions for $\mathbb{m}^{(\alpha)}$

While the main text defines $\mathbb{m}^{(\alpha)}$ as a three-dimensional unit vector which points from the midpoint between a lipid phosphorus atom and glycerol C2 atom, to the midpoint between the terminal methyl atoms on the lipid tail, we can also define $\mathbb{m}^{(\alpha)}$ in a number of different ways to determine the effect this will have on our extracted moduli. This is especially important if one considers defining $\mathbb{m}^{(\alpha)}$ on coarse-grained or other less-detailed models where individual atoms may not exist. Thus we can define two alternate definitions of $\mathbb{m}^{(\alpha)}$ which stem directly from the headgroup phosphorus atom (definition A1) and directly from the glycerol backbone C2 atom (definition A2). The following two tables list various membrane moduli for definitions A1 and A2.

Table S4. Membrane moduli obtained using definition A1 (phosphorus to the mean point between terminal tail methyl atoms) for $\mathbb{m}^{(\alpha)}$, then compared to the values listed in Table 1. While the K_c differ by less than 2% from the definition used in the text, K_{tw} and K_θ vary by up to 18%.

	K_c^{A1} ($\times 10^{-20}$ J)	$K_c^{A1} - K_C$ ($\times 10^{-20}$ J)	K_θ^{A1}($\times 10^{-20}$ J/nm^2)	$K_\theta^{A1} - K_\theta$ ($\times 10^{-20}$ J/nm^2)	K_{tw}^{A1} ($\times 10^{-20}$ J)	$K_{tw}^{A1} - K_{tw}$ ($\times 10^{-20}$ J)
DPPC	15.9	0.3	5.6	0.7	2.3	0.3
DOPC	11.6	0.2	7.5	0.9	1.1	0.2
DOPE	11.3	-0.1	9.4	1.1	1.5	0.1

Table S5. Membrane moduli obtained using definition A2 (glycerol backbone C2 to the mean point between terminal tail methyl atoms) for $\mathbb{m}^{(\alpha)}$, then compared to the values listed in Table 1. Variation of modulii for DOPC and DOPE is similar to that obtained with definition A1 (Table S4). However K_c for DPPC differs from the definition in the text by 5%, and K_θ K_{tw} by up to 20%.

	K_c^{A2} ($\times 10^{-20}$ J)	$K_c^{A2} - K_C$ ($\times 10^{-20}$ J)	K_θ^{A2} ($\times 10^{-20}$ J/nm^2)	$K_\theta^{A2} - K_\theta$ ($\times 10^{-20}$ J/nm^2)	K_{tw}^{A2} ($\times 10^{-20}$ J)	$K_{tw}^{A2} - K_{tw}$ ($\times 10^{-20}$ J)
DPPC	14.8	-0.8	4.1	-0.8	1.7	-0.3
DOPC	10.9	-0.5	5.6	-1.0	0.8	-0.1
DOPE	11.3	-0.1	7.1	-1.2	1.3	-0.1

Calculation of Membrane Area per Lipid and K_A

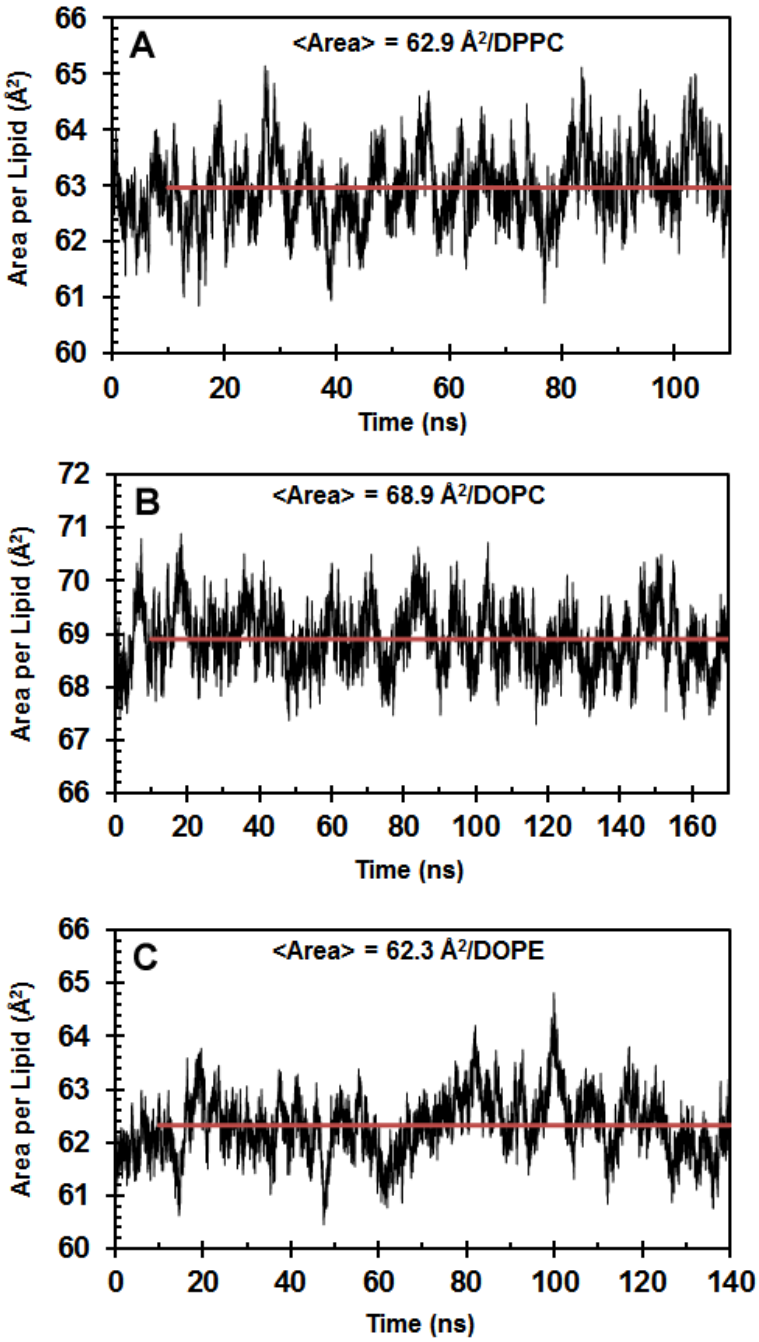

Figure S5. Area per lipid of a 648 DPPC (A), DOPC (B) and DOPE (C) bilayers using the CHARMM36 force field (first 10 ns ignored for averaging). Good convergence and stability for each system are evident.

K_A was estimated from the mean square fluctuation in membrane area $<\delta A^2>$ (Fig S5) using the relation:

$$< \delta A^2 > = < (A - A_0)^2 > = k_B T \left[\frac{\partial A}{\partial \gamma}\right]_T = \frac{k_B T A_0}{N K_A} \quad (S7)$$

where k_B is the Boltzmann constant, T is temperature, A_0 is the tensionless membrane area per lipid, and N is the number of lipids per monolayer leaflet (324 in this paper).

Alternate Analysis Methods and a Test of Box Size Dependence

Here we present two alternate methods to estimate K_c from molecular simulations, and compare the bending constants of DPPC extracted from systems of 288 and 648 lipids via the approach based on eq 2. Figure S6 and Tables S6-S8 elucidate how traditional Helfrich-Canham (HC) theory (eq 1) can be modified, based on eq 3, to yield estimates of K_c in small simulation boxes. Figure S7 and Table S9 present an analysis based on the local real-space analysis of lipid splay described by Khelashvili et. al.[4]. Fig. S8 repeats the analysis of Fig. 2 for DPPC for a smaller system than that presented in the main text.

It is clear in Fig. S6 that, for the simulation sizes considered in this work, the height spectra do not converge to the HC limit. The longer wavelength data does, however, converge to the extended HC result of eq 3 and this can be seen most easily by subtracting off the tilt contribution appearing in eq 3 using the tilt modulus obtained via analysis of the transverse fluctuations in eq 2. As was found for the coarse-grained systems studied in Ref. 3, exploiting this procedure to estimate K_c is highly sensitive to the molecular definition of $\mathbb{m}_j$. When carrying out the analysis for the definition of the main text (Table S6) and alternate definitions A1 and A2 (Tables S7 and S8), substantially different values of the bending modulus are obtained. The sensitivity of the tilt modulus to the definition of $\mathbb{m}_j$ (see tables S4 and S5) propagates into high uncertainties in the estimation of K_c. There is no such sensitivity of K_c to the definition of $\mathbb{m}_j$ when the analysis is carried out using eq2 (see tables S4 and S5).

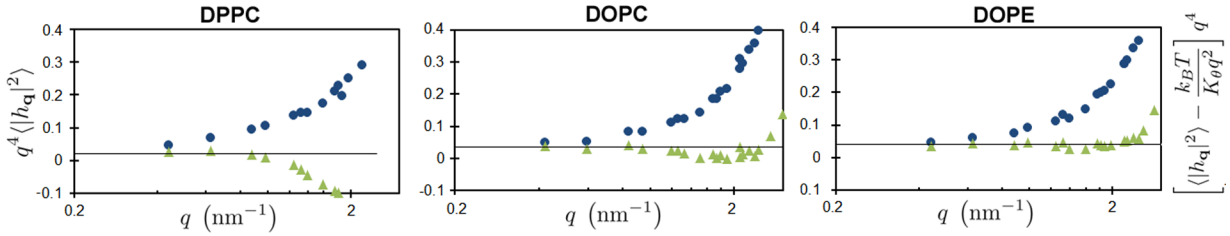

Figure S6. Power spectra of membrane height. In contrast to the longitudinal orientation spectra (Figure 2A-2C), the height spectra (blue circles and left y-axis label) are clearly not converged with respect to system size, making direct fits to eq 1 impossible. Converged spectra would exhibit a plateau regime at low q in these plots, as indicated by the horizontal black line. By subtracting the contribution from lipid tilting that appears in eq 3 convergence to a plateau regime can be obtained (green triangles and right y-axis label) from moderate-sized simulations, allowing estimation of K_c from eq 1.

Table S6. Membrane moduli obtained using corrected Helfrich-Canham (HC') spectra (eq 3) and a director definition employed in the main text ($\mathbb{m}_j$ begins between lipid phosphorus and glycerol C2).

	$K_c^{HC\prime}$ ($\times 10^{-20}$ J)	$K_c^{HC\prime} - K_C$ ($\times 10^{-20}$ J)
DPPC	13.0	-2.6
DOPC	11.6	0.2
DOPE	10.4	-1.0

Table S7. Membrane moduli obtained using corrected Helfrich-Canham (HC') spectra (eq 3) and director definition A1 ($\mathbb{m}_j$ begins from the lipid phosphorus atom).

	$K_c^{A1-HC'}$ ($\times 10^{-20}$ J)	$K_c^{A1-HC'}$ - K_C ($\times 10^{-20}$ J)
DPPC	11.0	-4.6
DOPC	10.5	-0.9
DOPE	9.8	-1.6

Table S8. Membrane moduli obtained using corrected Helfrich-Canham (HC') spectra (eq 3) and director definition A2 ($\mathbb{m}_j$ begins from the glycerol C2 atom).

	$K_c^{A2-HC'}$ ($\times 10^{-20}$ J)	$K_c^{A2-HC'}$ - K_C ($\times 10^{-20}$ J)
DPPC	19.0	3.4
DOPC	13.5	2.1
DOPE	11.3	-0.1

We next consider the local real-space analysis method of Khelashvili et al.[4]. This method extracts the potential of mean force associated with lipid-lipid orientational differences directly from simulation:

$$\mathrm{U} = -k_B T \ln\left[\frac{P(\alpha)}{\sin(\alpha)}\right] \quad \text{(S8)}$$

where α is the angle between two neighboring lipid directors, $\mathbb{m}_j$, and P(α) is the probability distribution of α over all time steps and all considered lipid pairs. To carry out the analysis, the authors specify that (a.) only lipid pairs separated by less than 1 nm be considered, and (b.) at least one director should be oriented less than or equal to 10 degrees from the bilayer normal or the lipid pair is excluded from analysis. By plotting eq S8 as a function of α, the monolayer bending constant K_m is extracted by fitting to the assumed functional form:

$$\mathrm{U} = \frac{1}{2} K_m \alpha^2 + \mathrm{Const.} \quad \text{(S9)}$$

over a limited set of small angles (10-30 degrees as specified in Ref. 4). K_c is then recovered as twice K_m. For consistency, we used the vector orientation definition provided by Khelashvili et al.[4], though they are similar to those defined in this manuscript. The results of this analysis are provided in Figure and Table S7. The results are in qualitative agreement, but differ by up to 17%, from the values obtained via analysis based on eq 2.

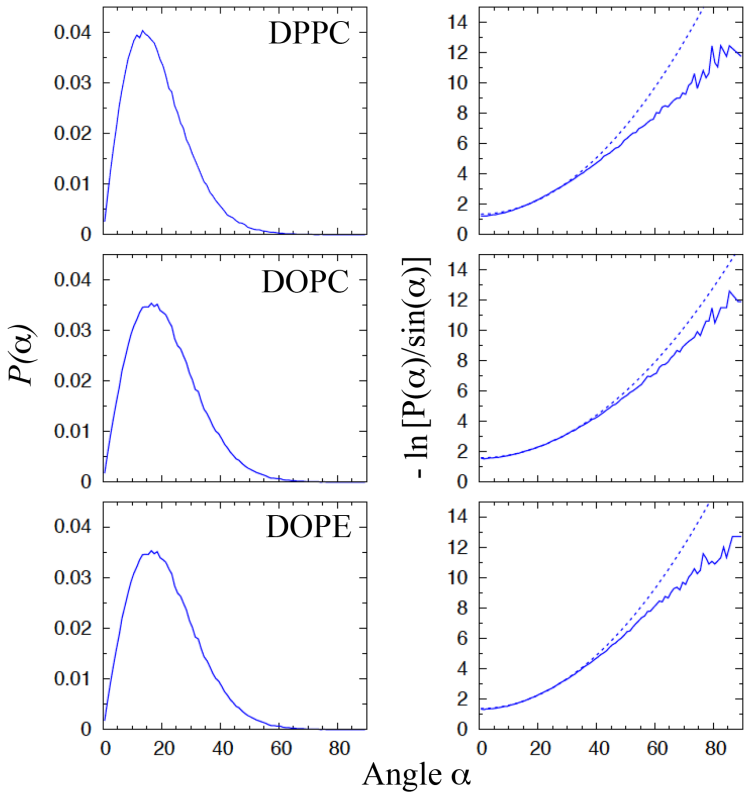

Figure S7. Angular distributions and potential of mean force (PMF) profiles used for the calculation of K_c in the methodology of Ref. 4. [LEFT] Normalized distributions of α between local director pairs for the three systems studied in this paper. [RIGHT] Associated PMF profiles that follow eq S8 (solid), overlaid with the best-fit results of eq S9 (dotted). Using the best fit of eq S9, K_c was extracted for each system and is listed in Table S7.

Table S9. Membrane bending moduli obtained using the method of Khelashvili et al.[3] Standard statistical errors are approximately 0.1 x 10^{-20} J. However, shifting the range that Eq (S9) is fit from [10-30 degrees] to [10-20], [20-30], [5-30], [10-35], and [5-35] degrees changes the calculated bending constants by approximately 5%.

	K_c^{Khel} (× 10^{-20} J)	K_c^{Khel} - K_C (× 10^{-20} J)
DPPC	13.6	-2.0
DOPC	9.5	-1.9
DOPE	11.8	0.4

Lastly, to investigate the effect of box size on the evaluation of K_c, a smaller all-atom DPPC system consisting of 288 lipids was considered. This system was run for 230 ns, and only the final 200 ns were analyzed. System conditions were identical to those reported earlier. Fig S8 below shows that the longitudinal orientation spectra for the smallest wavevectors converges to almost identical values as the 648 lipid data presented in Fig. 2. This validates our methodology in smaller systems and suggests that all-atom membranes as small as ¼ of our current 648 lipid system might be useful for calculating K_c.

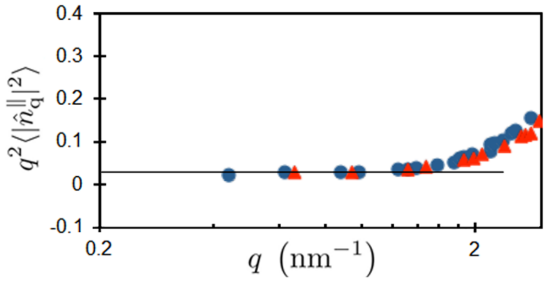

Figure S8. Power spectra of longitudinal lipid orientation weighted by q^2 for an all-atom 648 DPPC system (blue circles) and an all-atom 288 DPPC system (red triangles). In both cases, a clear convergence can be observed at low wavevectors which allows K_c to be extracted from eq 2. While the sizes of these systems are different from one another, the smaller system yields K_c = 15.1 ± 0.4 (x 10^{-20} J) which is within the standard error for the large system - 15.6 ± 0.5 (x 10^{-20} J) (Table 1). There is no noticeable effect of box size in the simulations, so long as the simulation size is large enough to reach the predicted plateau regime.

References

(1) Hynninen, A. P.; Crowley, M. F. *Journal of Computational Chemistry* **2014**, *35*, 406.
(2) Watson, M. C.; Penev, E. S.; Welch, P. M.; Brown, F. L. H. *Journal of Chemical Physics* **2011**, *135*, *244701*.
(3) Watson, M.C.; Brandt, E. G., Welch, P. M., Brown, F. L. H. *Phys. Rev. Lett.* **2012**, 109, 028102.
(4) Khelashvili, G.; Kollmitzer, B.; Heftberger, P.; Pabst, G.; Harries, D. *Journal of Chemical Theory and Computation* **2013**, *9*, 3866.